Androgen receptor coordinates muscle metabolic and contractile functions

Kamar Ghaibour, Mélanie Schuh, Sirine Souali-crespo, Céline Chambon, Anouk Charlot, Joe Rizk, Daniela Rovito, Anna-isavella Rerra, Qingshuang Cai, Nadia Messaddeq, et al.

ORIGINAL ARTICLE

Journal of Cachexia, Sarcopenia and Muscle 2023; **14**: 1707–1720
Published online 20 May 2023 in Wiley Online Library (wileyonlinelibrary.com) **DOI:** 10.1002/jcsm.13251

Androgen receptor coordinates muscle metabolic and contractile functions

Kamar Ghaibour[1], Mélanie Schuh[1], Sirine Souali-Crespo[1], Céline Chambon[1], Anouk Charlot[2], Joe Rizk[1], Daniela Rovito[1], Anna-Isavella Rerra[1], Qingshuang Cai[1], Nadia Messaddeq[1], Joffrey Zoll[2], Delphine Duteil[1]* & Daniel Metzger[1]*

[1]*Université de Strasbourg, CNRS, Inserm, IGBMC UMR 7104-UMR-S 1258, Illkirch, France;* [2]*Centre de Recherche de Biomédecine de Strasbourg, UR 3072 Mitochondrie, Stress Oxydant et Protection Musculaire, Université de Strasbourg, Strasbourg, France*

Abstract

Background Androgens are anabolic steroid hormones that exert their function by binding to the androgen receptor (AR). We have previously established that AR deficiency in limb muscles impairs sarcomere myofibrillar organization and decreases muscle strength in male mice. However, despite numerous studies performed in men and rodents, the signalling pathways controlled by androgens via their receptor in skeletal muscles remain poorly understood.

Methods Male $AR^{skm-/y}$ ($n = 7$–12) and female $AR^{skm-/-}$ mice ($n = 9$), in which AR is selectively ablated in myofibres of musculoskeletal tissue, and male $AR^{(i)skm-/y}$, in which AR is selectively ablated in post-mitotic skeletal muscle myofibres ($n = 6$), were generated. Longitudinal monitoring of body weight, blood glucose, insulin, lipids and lipoproteins was performed, alongside metabolomic analyses. Glucose metabolism was evaluated in C2C12 cells treated with 5α-dihydrotestosterone (DHT) and the anti-androgen flutamide ($n = 6$). Histological analyses on macroscopic and ultrastructural levels of longitudinal and transversal muscle sections were conducted. The transcriptome of gastrocnemius muscles from control and $AR^{skm-/y}$ mice was analysed at the age of 9 weeks ($P < 0.05$, 2138 differentially expressed genes) and validated by RT-qPCR analysis. The AR (4691 peaks with false discovery rate [FDR] < 0.1) and H3K4me2 (47 225 peaks with FDR < 0.05) cistromes in limb muscles were determined in 11-week-old wild-type mice.

Results We show that disrupting the androgen/AR axis impairs in vivo glycolytic activity and fastens the development of type 2 diabetes in male, but not in female mice. In agreement, treatment with DHT increases glycolysis in C2C12 myotubes by 30%, whereas flutamide has an opposite effect. Fatty acids are less efficiently metabolized in skeletal muscles of $AR^{skm-/y}$ mice and accumulate in cytoplasm, despite increased transcript levels of genes encoding key enzymes of beta-oxidation and mitochondrial content. Impaired glucose and fatty acid metabolism in AR-deficient muscle fibres is associated with 30% increased lysine and branched-chain amino acid catabolism, decreased polyamine biosynthesis and disrupted glutamate transamination. This metabolic switch generates ammonia (2-fold increase) and oxidative stress (30% increased H_2O_2 levels), which impacts mitochondrial functions and causes necrosis in <1% fibres. We unravel that AR directly activates the transcription of genes involved in glycolysis, oxidative metabolism and muscle contraction.

Conclusions Our study provides important insights into diseases caused by impaired AR function in musculoskeletal system and delivers a deeper understanding of skeletal muscle pathophysiological dynamics that is instrumental to develop effective treatment for muscle disorders.

Keywords androgen receptor; genomics; metabolism; skeletal muscle; type 2 diabetes

Received: 23 December 2022; Revised: 8 April 2023; Accepted: 15 April 2023
**Correspondence to: Delphine Duteil and Daniel Metzger, Université de Strasbourg, CNRS, Inserm, IGBMC UMR 7104-UMR-S 1258, F-67400 Illkirch, France. Email: duteild@igbmc.fr and metzger@igbmc.fr*
Kamar Ghaibour and Mélanie Schuh equally contributed.

Introduction

Skeletal muscle is a dynamic tissue essential for posture, locomotion and energy balance in mammals. It is composed of myofibres with different contractile and metabolic properties. Slow-twitch muscles preferentially use fatty acids that are metabolized by beta-oxidation for ATP production, whereas fast-twitch ones mainly generate energy via glycolysis.[1] Most limb muscles (e.g., gastrocnemius, tibialis and quadriceps) are composed of both oxidative and glycolytic fibres and have the capacity to switch between oxidative and glycolytic metabolism in response to environmental demands. For instance, endurance exercise induces fibre type switching from fast glycolytic to slow oxidative,[2] whereas sedentariness decreases muscle oxidative capacities,[3] associated with oxidative stress,[4] as well as obesity and type 2 diabetes.[5]

Hormones, such as thyroid hormones, glucocorticoids and sex hormones, also play an important role in muscle function and metabolic plasticity.[6–9] In particular, increased testosterone levels at puberty in males promote muscle mass and strength[6,10] and stimulate glucose metabolism in skeletal muscle.[11] Androgen effects are mediated by the androgen receptor (AR; NR3C4), which belongs to the nuclear receptor superfamily.[12] Even though AR is expressed in both males and females,[13] the later produce low testosterone levels.[14] AR overexpression in skeletal muscles of male mice increases lean and reduces fat mass. This shift in body composition is associated with fast myofibre hypertrophy and enhanced muscle mitochondrial activity.[15] Conversely, AR inhibition impairs fat metabolism in skeletal muscle by reducing the expression of the fatty acid transporter CD36.[16] Our previous study showed that the androgen-dependent postnatal growth of perineal muscles is mediated by myofibre AR, whereas that of limb muscles is myofibre AR independent.[17] However, AR deficiency in limb muscles impairs myofibrillar organization and decreases muscle strength, demonstrating that AR controls critical pathways required for force production.[17,18] Nevertheless, despite numerous studies performed in humans[19] and rodents,[11,15–18,20] the molecular and cellular mechanisms by which androgens via their receptor affect limb myofibre homeostasis remain poorly understood. Here, we show that myofibre AR controls the expression of numerous genes encoding key proteins involved in muscle contraction and metabolic enzymes. Myofibre AR depletion impairs glucose and fatty acid oxidation and promotes amino acid catabolism, resulting in oxidative stress, mitochondria dysfunction and myofibre necrosis in the most affected fibres, and it hastens the development of type 2 diabetes.

Materials and methods

Study approval

All mouse experiments were done in an accredited animal house, in compliance with French and EU regulations on the use of laboratory animals for research. Intended manipulations were submitted to the ethics committee (Com'Eth, Strasbourg, France) and to the French Research Ministry (MESR) for ethical evaluation and authorization according to the 2010/63/EU directive under the APAFIS numbers 2012-025, 2012-027, 2012-028 and 23910.

Mouse studies

$AR^{skm-/y}$ mice were previously described.[17] In brief, $AR^{L2/y}$ mice[21] were intercrossed with HSA-Cre mice that express the Cre recombinase selectively in skeletal muscle myofibres,[22] to generate control ($AR^{L2/y}$) and $AR^{skm-/y}$ mutant male mice, as well as control ($AR^{L2/L2}$) and $AR^{skm-/-}$ mutant female mice. Alternatively, $AR^{L2/y}$ mice were intercrossed with HSA-$CreER^{T2}$ mice that express the tamoxifen-dependent $CreER^{T2}$ recombinase in myofibres.[23] Seven-week-old $AR^{L2/y}$ control male mice and sex-matched HSA-Cre-ER^{T2}/$AR^{L2/y}$ somatic pre-mutant littermates were intraperitoneally injected with tamoxifen (1 mg/day) for 5 days to generate control and $AR^{(i)skm-/y}$ mutant mice, respectively, as described.[17] All mice were on a C57BL/6J background.

Mice were maintained in a temperature- and humidity-controlled animal facility, with a 12-h light/dark cycle. Water and standard rodent chow (2800 kcal/kg, Usine d'Alimentation Rationnelle, Villemoisson-sur-Orge, France) were provided ad libitum. Breeding and maintenance of mice were performed according to institutional guidelines.

Body weight was determined every week. Food and water consumption were measured with a Labmaster system (TSE, www.TSE-Systems.com) at 26-min intervals for 24 h. The data presented are the 24-h average. Body lean and fat content were recorded in anaesthetized mice by qNMR (PIXIMUS, GE Medical Systems) according to the manufacturer's instructions.[5] Animals were sacrificed between 9 and 11 AM by cervical dislocation, and tissues were immediately collected, weighed and frozen in liquid nitrogen or processed for biochemical and histological analyses.

Statistics

Significance was calculated with GraphPad Prism (www.graphpad.com, GraphPad Software) using the two-tailed Mann–Whitney test and Student's *t*-test, one-way analysis of variance (ANOVA) or two-way ANOVA.

Data availability

RNA-seq (GSE216372) and ChIP-seq (GSE216373) data reported in this study are available on Gene Expression Omnibus (GEO) database.

See supporting information for histological, blood and serum analyses, metabolic enzyme activity and ammonium content measurements, quantification of mitochondrial and nuclear DNA content, metabolomics analysis, cell culture, protein analysis, mitochondria respiration and H_2O_2 production analysis, RNA extraction and quantification, and chromatin immunoprecipitation.

Results

Myofibre androgen receptor deficiency impairs glycolysis in limb muscles and promotes type 2 diabetes in male mice

To provide insights on androgen signalling in skeletal muscle, we first determined AR levels in gastrocnemius of sedentary male mice. Western blot analysis revealed that they culminate between 11 and 15 weeks of age (*Figure 1A,B*). Interestingly, after 15 weeks, limb muscles undergo an oxidative-to-glycolytic switch,[5] associated with glucose intolerance and insulin resistance (*Figure S1A,B*). To determine the role of AR in muscle metabolism, we analysed $AR^{skm-/y}$ mice, in which AR is selectively knocked out in myofibres.[17] In agreement with our previous results,[17] western blot and immunofluorescent analyses revealed that AR was efficiently ablated in skeletal muscle fibres, but not in satellite cells (*Figure S1C–E*). Water and food intake (*Figure S1F*), and lean and fat content (*Figure S1G*) were similar in $AR^{skm-/y}$ and control mice at the age of 15 weeks. Moreover, even though AR ablation in myofibres did not affect the body weight over a 30-week period (*Figure S1H*), blood glucose levels were higher in $AR^{skm-/y}$ mice than those in control littermates between 10 and 25 weeks (*Figure 1C*), and intraperitoneal glucose tolerance tests (IPGTTs) showed that mice lacking myofibre AR became glucose intolerant at 15 weeks of age (*Figure 1D*). In addition, blood insulin levels were higher in $AR^{skm-/y}$ mice than those in controls at 15 and 25 weeks (*Figure 1E*), and intraperitoneal insulin sensitivity tests (IPISTs) revealed that $AR^{skm-/y}$ mice became insulin resistant earlier than their control littermates (*Figure 1F*), indicating that muscle glycolytic pathways are impaired in the absence of myofibre AR in males. Note that glucose metabolism was also impaired in $AR^{(i)skm-/y}$ mice, in which AR was selectively ablated in skeletal myofibres at adulthood (*Figure S2A–D*), despite a similar body weight (*Figure S2E*). In contrast, $AR^{skm-/-}$ female mice had similar body weight and blood glucose levels compared with controls between 7 and 20 weeks (*Figure S3A–C*) and were not glucose intolerant at 20 weeks (*Figure S3D*). Thus, AR controls key metabolic functions in mature myofibres after puberty selectively in males.

Interestingly, the activity of hexokinase (HK), the rate-limiting enzyme of glycolysis, was decreased by 20% in quadriceps muscles of 15-week-old $AR^{skm-/y}$ male mice (*Figure 2A*), and western blot analysis showed that protein levels of HK2 follow those of AR with age, reaching a peak between 11 and 13 weeks (*Figure 1A,B*). To provide further insights on the role of androgens in glucose metabolism, we evaluated its uptake in C2C12 myotubes. 5α-Dihydrotestosterone (DHT) induced AR levels (*Figure S4*) and enhanced the incorporation of 2-deoxyglucose (2-DG), a glucose analogue that cannot be metabolized (*Figure 2B*). Conversely, the AR-selective non-steroidal anti-androgen flutamide lowered 2-DG uptake by 20% (*Figure 2B*). Extracellular acidification rate (ECAR) measurements revealed that glycolysis, maximal glycolytic capacities and glycolytic reserve were decreased by flutamide (*Figure 2C,D*), whereas DHT had an opposite effect (*Figure 2E,F*), demonstrating that androgens via AR stimulate the glycolytic activity in C2C12 myotubes. Altogether, these data show that AR deficiency in myofibres impairs glucose uptake and glycolytic capacities and leads to the development of type 2 diabetes at earlier time in $AR^{skm-/y}$ mice than in control male mice, without impacting adiposity.

Oxidative metabolism is impaired in skeletal muscles of $AR^{skm-/y}$ mice

Even though glucose metabolism was altered in $AR^{skm-/y}$ mice after 15 weeks, their cholesterol and triglyceride blood levels were similar to those of control mice at 15 and 25 weeks (*Figure S5A,B*). Free fatty acid (FFA) levels were also alike in control and $AR^{skm-/y}$ mice at 15 weeks and increased with age in controls but not in mutants (*Figure 3A*). Transcript levels of the fatty acid transporter *Cd36* were 30% higher in gastrocnemius muscles of 15-week-old $AR^{skm-/y}$ mice than in those of age-matched control mice (*Figure 3B*), indicating that FFA uptake might be increased in muscles of $AR^{skm-/y}$ mice. Furthermore, the transcript levels of genes encoding key enzymes of beta-oxidation (*Acox1*, *Acads*, *Acadl*, *Echs1*

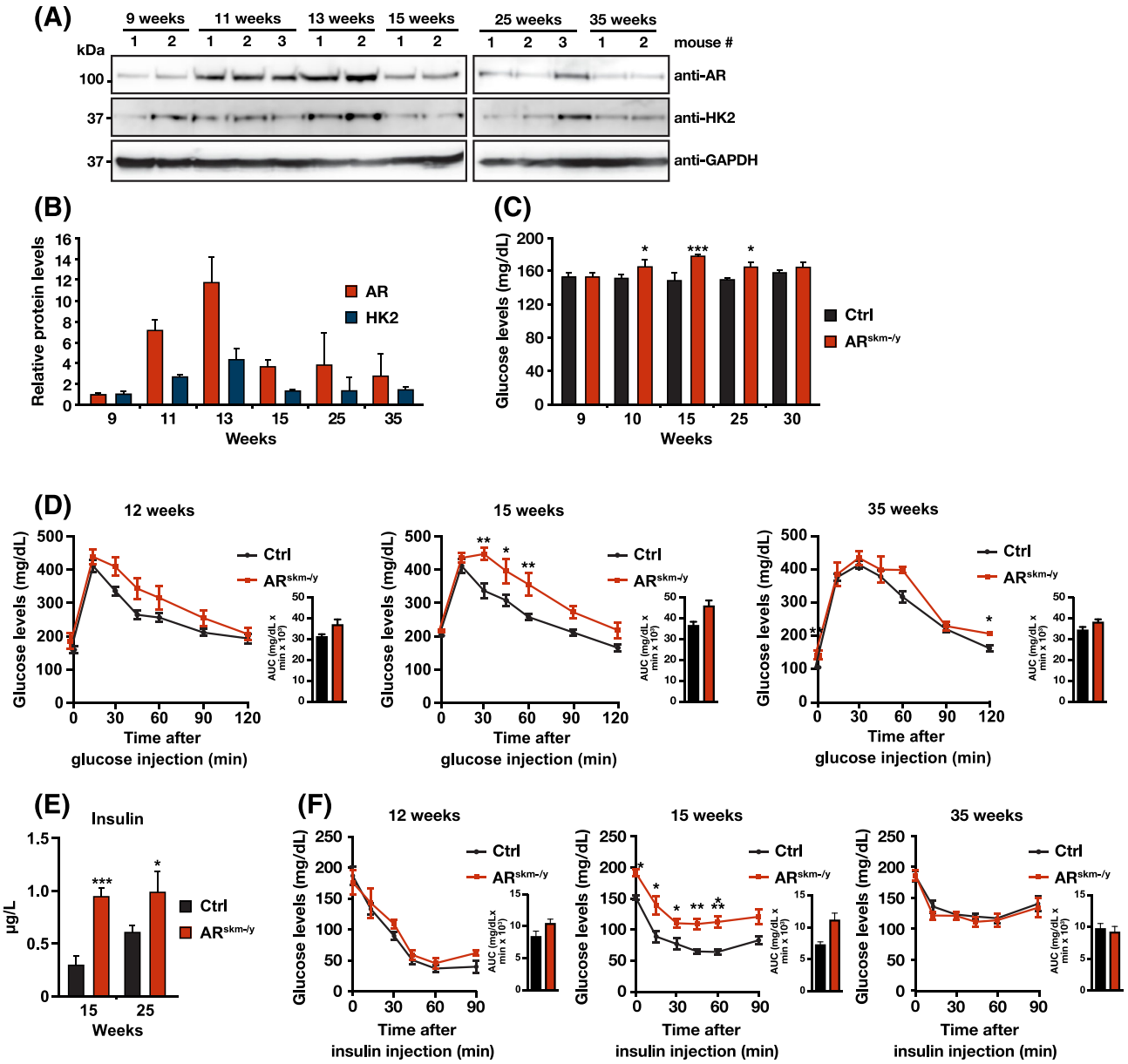

Figure 1 Role of myofibre androgen receptor (AR) in glucose metabolism of male mice (see also *Figures S1–S3*). (A, B) Representative western blot analysis (A) and quantification (B) of AR and hexokinase 2 (HK2) protein levels in gastrocnemius muscle of 9- to 35-week-old C57BL/6J male mice. GAPDH was used as a loading control. n = 2–3 mice per time point. Western blot performed in duplicate. (B) Mean + SEM. (C–F) Basal blood glucose levels (C), intraperitoneal glucose tolerance test (IPGTT) (D), blood insulin levels (E) and intraperitoneal insulin sensitivity test (IPIST) (F) of control (Ctrl) and $AR^{skm-/y}$ mice at indicated ages. The areas under the curve (AUCs) of IPGTT and IPIST experiments are presented next to each panel. (C) n = 8 Ctrl and 12 $AR^{skm-/y}$ mice. (D, F) n = 7 Ctrl and $AR^{skm-/y}$ mice. (E) n = 7 Ctrl and 12 $AR^{skm-/y}$ mice at 15 weeks, and n = 12 Ctrl and 8 $AR^{skm-/y}$ mice at 25 weeks. (C, E) Mean + SEM. (D, F) Mean ± SEM. (C, E) Two-tailed t-test. (D, F) Two-way ANOVA with Sidak's correction. $^{*}P < 0.05$, $^{**}P < 0.01$ and $^{***}P < 0.001$.

and *Hadhb*; *Figure 3B*) were enhanced in mutant mice. In addition, mitochondrial content, determined by qPCR analysis conducted on mitochondrial and genomic DNA, was slightly higher in quadriceps and tibialis of mutant mice (*Figures 3C* and *S5C*). Moreover, ultrastructural analysis revealed that interfibrillar mitochondrial cross-section area was higher in tibialis of $AR^{skm-/y}$ mice than that of control ones (*Figure 3D–F*).

To be processed by beta-oxidation, fatty acids are cleaved by lipases to generate fatty-acyl CoA (FA-CoA), which is complexed with carnitine in the cytoplasm and imported in the mitochondria by CPT1A, the activity of which is inhibited by malonyl-CoA. Malonyl-CoA is produced from acetyl-CoA by the acetyl-CoA carboxylase (ACC) that is inhibited by phosphorylation.[24] Our analyses revealed that the expression and activity of the triglyceride hydrolase lipoprotein lipase

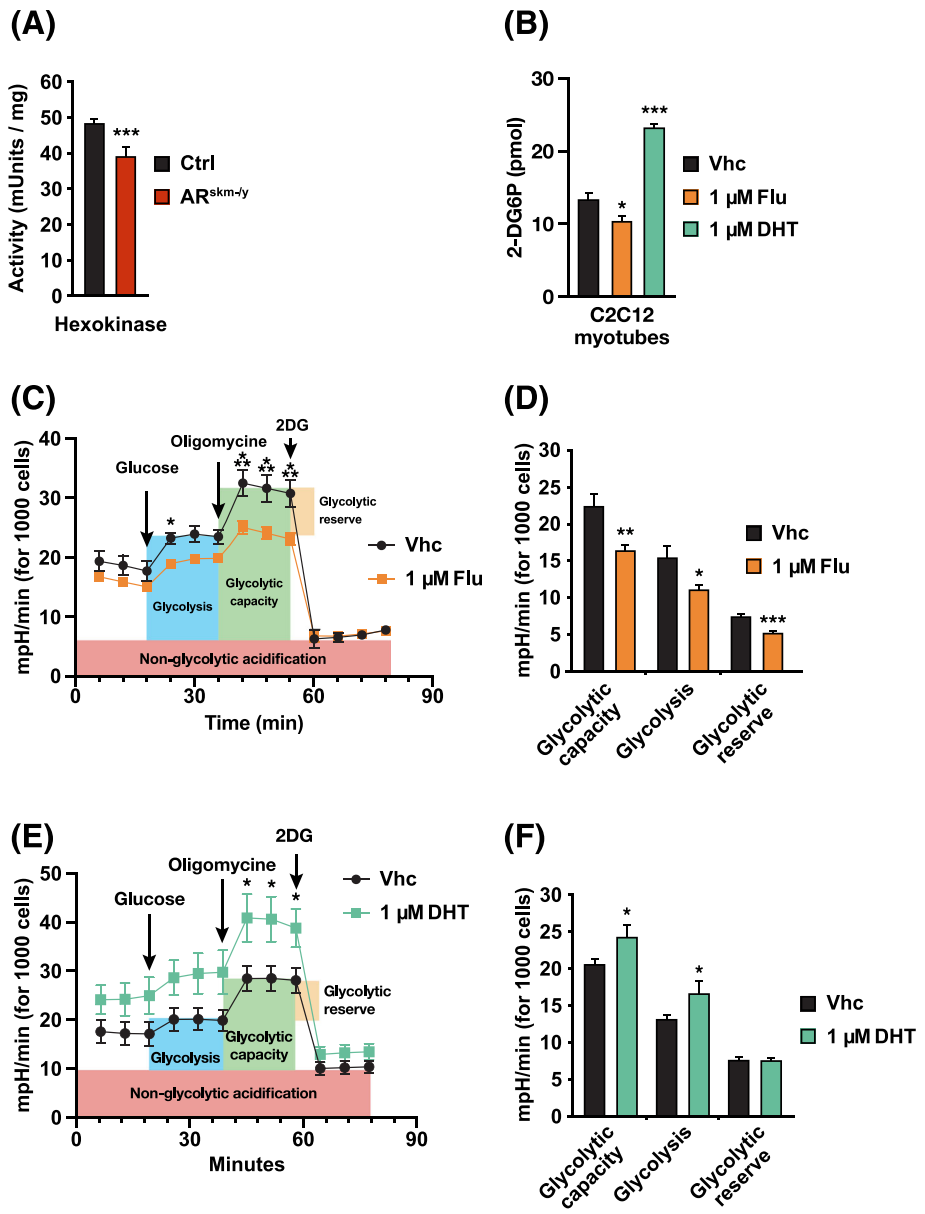

Figure 2 Role of androgen receptor (AR) in myofibre glycolytic activity (see also *Figure S4*). (A) Hexokinase activity in quadriceps muscles of control and $AR^{skm-/y}$ mice at 15 weeks of age. $n = 4$. Mean + SEM. Two-tailed Mann–Whitney test. $^{***}P < 0.001$. (B–F) 2-Deoxyglucose (2-DG) uptake (B), representative extracellular acidification rate (ECAR) (C, E) and maximal glycolytic capacity, glycolysis and glycolytic reserve deduced from ECAR (D, F) in C2C12 myotubes treated with 1 µM of flutamide (Flu), 1 µM of 5α-dihydrotestosterone (DHT) or with vehicle (Vhc). (B) $n = 3$, (C–F) $n = 6$. (B, D, F) Mean + SEM. (C, E) Mean ± SEM. (B) One-way ANOVA with Dunnett's correction. (C, E) Two-way ANOVA with Sidak's correction. (D, F) Two-tailed *t*-test. $^{*}P < 0.05$, $^{**}P < 0.01$ and $^{***}P < 0.001$.

(LPL) were decreased in quadriceps muscle of $AR^{skm-/y}$ mice (*Figure 4A,B*) and that the transcripts levels of *Pnpla2*, encoding the lipase adipose triglyceride lipase (ATGL) that catalyses the conversion of triacylglycerides to diacylglycerides and FA-CoA, were lower in the absence of myofibre AR (*Figure 4A*), indicating decreased lipolysis and FA-CoA production. Moreover, metabolomic analysis revealed increased levels of free carnitine (i.e., not complexed with FA-CoA) in myofibres lacking AR (*Figure 4C*). In addition, western blot analysis unveiled that the ratio between phosphorylated and total ACCs was decreased by two-fold in gastrocnemius muscle of $AR^{skm-/y}$ mice (*Figure 4D,E*), indicating that CPT1A activity is impaired and that FA-CoA import to the mitochondria might be reduced. In agreement with these results, ultrastructural analyses revealed the presence of a higher number of lipid droplets in myofibres of $AR^{skm-/y}$ mice than in controls (*Figures 4F* and *S5D*). Together, these data show that the uptake of FA is enhanced in skeletal muscles of $AR^{skm-/y}$

DOI: 10.1002/jcsm.13251

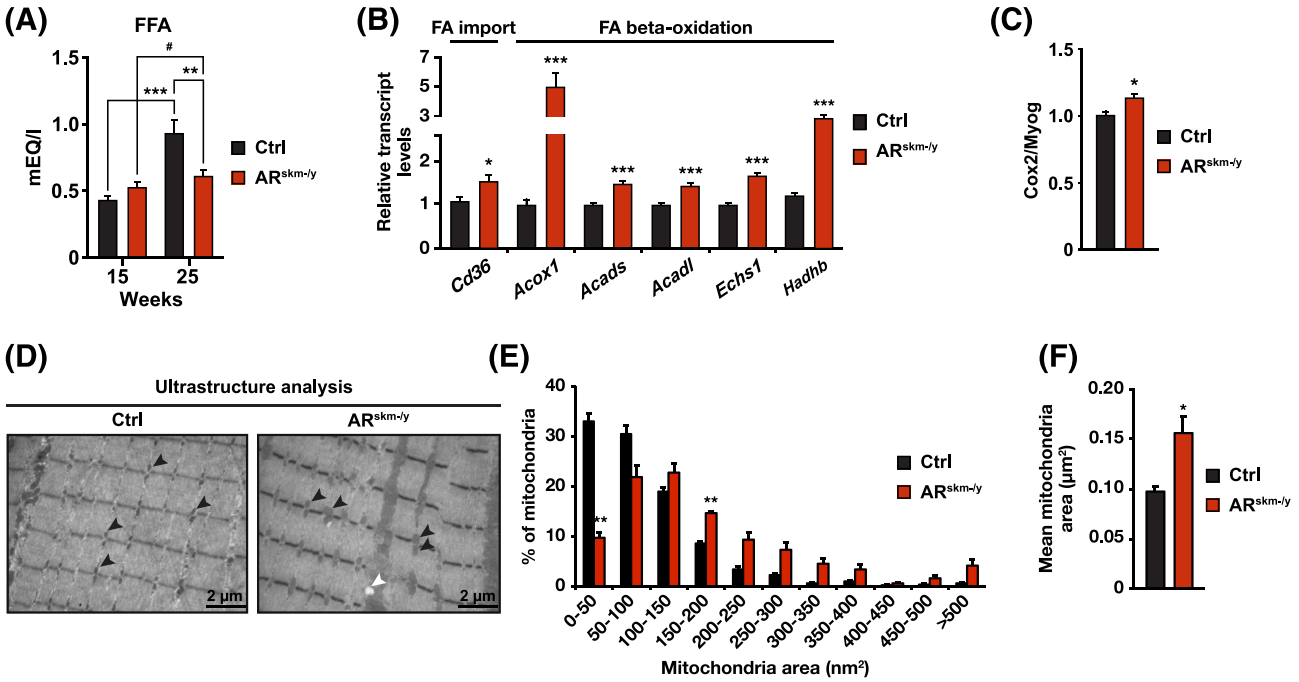

Figure 3 Role of myofibre androgen receptor (AR) in fatty acid metabolism (see also *Figure S5*). (A) Blood free fatty acid (FFA) content in control (Ctrl) and $AR^{skm-/y}$ mice at indicated ages. n = 7 Ctrl and 12 $AR^{skm-/y}$ mice at 15 weeks, and n = 12 Ctrl and 8 $AR^{skm-/y}$ mice at 25 weeks. Mean + SEM. Two-way ANOVA with Sidak's correction. #Non-significant, $^{**}P < 0.01$ and $^{***}P < 0.001$. (B) Relative transcript levels of indicated genes in gastrocnemius muscles of 15-week-old Ctrl and $AR^{skm-/y}$ mice. n = 6 mice, mean + SEM, two-tailed t-test. $^{*}P < 0.05$ and $^{***}P < 0.001$. (C) Quantification of mitochondrial content in quadriceps muscles of 15-week-old Ctrl and $AR^{skm-/y}$ mice by qPCR amplification of the *Cox2* mitochondrial-encoded gene and the *Myog* nuclear-encoded gene. n = 6 mice. Mean + SEM. Two-tailed t-test. $^{*}P < 0.05$. (D) Representative ultrastructure of tibialis muscles of 15-week-old Ctrl and $AR^{skm-/y}$ mice. White arrowheads show lipid accumulation and black arrowheads point to mitochondria. Scale bar: 2 µm. n = 10 mice, 10 fields per mouse. (E, F) Distribution (E) and average (F) of mitochondrial cross-section area in tibialis muscles of 15-week-old Ctrl and $AR^{skm-/y}$ mice. n = 4 mice, 4 fields per mouse. (E, F) Mean + SEM. (E) Two-way ANOVA with Sidak's correction. (F) Two-tailed Mann–Whitney test. $^{*}P < 0.05$ and $^{**}P < 0.01$.

mice, whereas their metabolism is impaired, despite enhanced transcript levels of genes encoding beta-oxidation enzymes, resulting in their accumulation in cytoplasm.

Loss of myofibre androgen receptor promotes amino acid catabolism and oxidative stress

Amino acids constitute an alternative source of energy in muscles. Indeed, branched-chain amino acids (BCAAs; leucine, isoleucine and valine) can be converted to acetyl-CoA, and asparagine, aspartate and glutamate can be catabolized into intermediates of the tricarboxylic acid (TCA) cycle.[25] Because both glucose and fatty acid processing were impaired upon AR loss, we investigated whether amino acid metabolism was affected in muscles. Metabolomic analysis of the amino acid content in gastrocnemius muscles of 15-week-old mice revealed decreased levels of lysine, leucine, isoleucine and valine in $AR^{skm-/y}$ mice, even though those of the latter did not reach statistical significance (*Figures 5A* and *S6A*). In agreement with these results, transcript levels of the rate-limiting enzyme of BCAA catabolism *Bcat2*, as well as those of *Echs1*, *Acads* and *Hadhb*, encoding enzymes involved in BCAA and lysine degradation, as well as in beta-oxidation, were increased in mutant muscles (*Figures 3B* and *5B*). BCAT2 converts alpha-glutamate into glutamate, which can be metabolized into ornithine via ALDH18A1 and OAT to integrate the polyamine pathway,[26] or can be interconverted into alpha-ketoglutarate by glutamate dehydrogenase (GLUD1), with the production of NH_3[27] (*Figure S6B*). Even though *Aldh18a1* transcript levels were similar in gastrocnemius of $AR^{skm-/y}$ and control mice, those of *Oat* and those encoding key enzymes involved in polyamine interconversion (i.e., *Odc1*, *Smox* and *Amd1*) were decreased in the absence of myofibre AR (*Figure 5B*), indicating that glutamate might less efficiently integrate the polyamine pathway. In agreement, our metabolomic analyses revealed that glutamate amounts rose by 1.8-fold in muscles of $AR^{skm-/y}$ mice (*Figure 5C*), even though the transcript levels of *Glud1* were increased in the absence of myofibre AR (*Figure 5B*). As expected, higher *Glud1* expression was accompanied by a two-fold increase in NH_3 content in quadriceps muscle of $AR^{skm-/y}$ mice (*Figure 5D*). Because previous studies showed that ammonia excess impairs skeletal muscle mitochondrial activity,[28] we determined ammonia levels in saponin-skinned fibres of gastrocnemius from 15-week-old

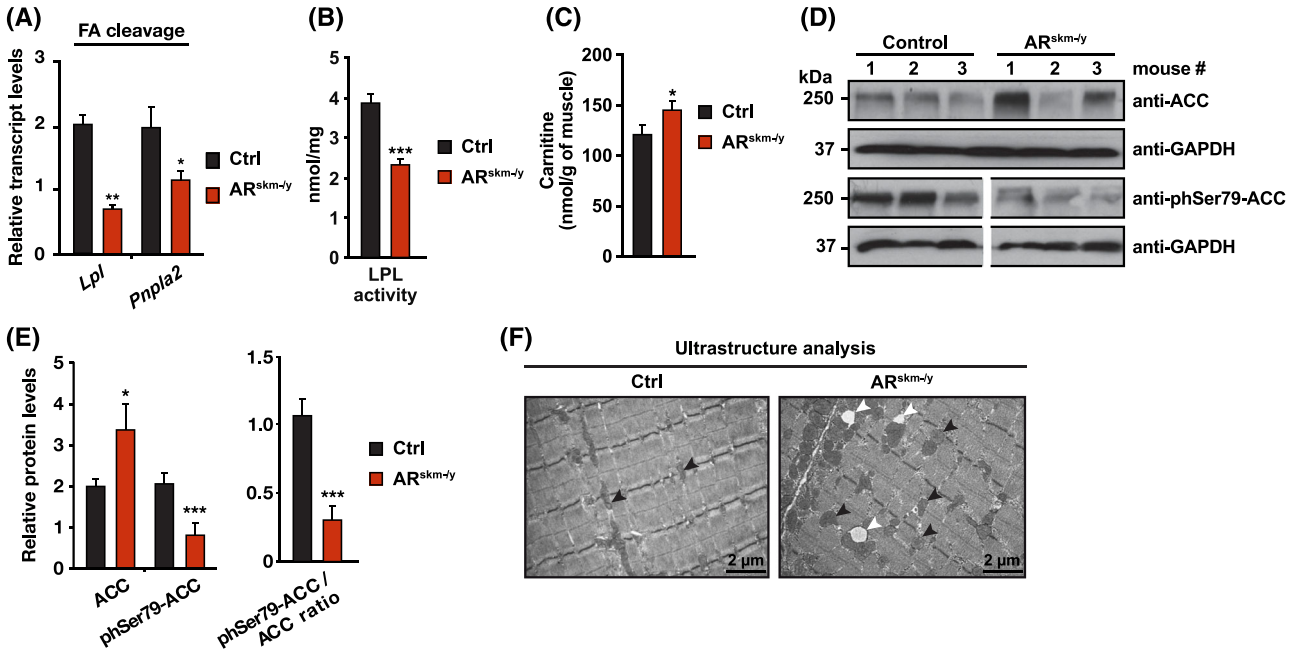

Figure 4 Role of myofibre androgen receptor (AR) in oxidative metabolism (see also *Figure S5*). (A) Relative transcript levels of indicated genes in gastrocnemius muscles of 15-week-old control (Ctrl) and $AR^{skm-/y}$ mice. $n = 6$ mice. Mean + SEM. Two-tailed *t*-test. $*P < 0.05$ and $**P < 0.01$. (B) Lipoprotein lipase (LPL) activity in quadriceps muscles of Ctrl and $AR^{skm-/y}$ mice at 15 weeks of age. $n = 4$ mice. Mean + SEM. Two-tailed Mann–Whitney test. $***P < 0.001$. (C) Free carnitine levels in gastrocnemius muscles of 15-week-old Ctrl and $AR^{skm-/y}$ mice. $n = 3$ mice. Mean + SEM. Two-tailed Mann–Whitney test. $*P < 0.05$. (D, E) Representative western blot analysis of total and phosphorylated acetyl-CoA carboxylases (ACCs) (D), corresponding protein quantification and ratio between the phosphorylated and total ACC protein contents (E) in gastrocnemius muscle of 15-week-old Ctrl and $AR^{skm-/-}$ mice. GAPDH was used as a loading control. $n = 7$ mice. Mean + SEM. Two-tailed *t*-test. $*P < 0.05$ and $***P < 0.001$. (F) Representative ultrastructure of gastrocnemius muscles of 15-week-old Ctrl and $AR^{skm-/y}$ mice. White arrowheads show lipid accumulation and black arrowheads point to mitochondria. Scale bar: 2 µm. $n = 10$ mice, 10 fields per mouse.

mice. In the presence of the mitochondrial substrates' pyruvate/malate and ADP (complex I, III, IV and V activities), oxygen (O_2) consumption was 33% lower in fibres of $AR^{skm-/y}$ mice than that of control mice (*Figure 5E*, Vadp). Moreover, the maximal speed of respiration assessed by succinate supplementation (Vsucc) and Vrot (complexes II–V), determined after blocking complex I with rotenone, was lower in myofibres lacking AR (*Figure 5E*), indicating that the activity of terminal complexes might be affected. In accordance, staining for Cox activity (complex IV) in quadriceps muscle revealed that the percentage of dark oxidative fibres was decreased in the absence of myofibre AR (*Figure 5F*), showing that the activity of oxidative phosphorylation terminal complexes is lower. As impaired mitochondrial activity might result in increased reactive oxygen species (ROS) production, we recorded H_2O_2 flux during mitochondrial respiration and found higher levels in myofibres in the absence of AR (*Figure 6A*). These results were corroborated by enhanced fluorescence intensity of dihydroethidium (DHE; a probe that detects ROS) (*Figure 6B*), showing that oxidative stress is increased in muscles of $AR^{skm-/y}$ mice.

Metabolomics studies also uncovered that levels of carnosine, a dipeptide of beta-alanine and histidine that scavenges ROS and buffers pH in muscle cells, were decreased in gastrocnemius muscles of $AR^{skm-/y}$ mice (*Figure 6C*), whereas those of methionine sulfoxide (MetO), the oxidized form of the amino acid methionine, were increased (*Figure 6D*). Of note, transcript levels of *Msrb3*, which encodes the most abundant isoform of the methionine sulfoxide reductase (MSR) in skeletal muscle that catalyses the reduction of toxic oxidized methionine residues, thereby scavenging ROS, were decreased in the absence of AR (*Figure 6E*). Thus, these data show that ROS production is enhanced in muscles of $AR^{skm-/y}$ mice, whereas their scavenging is reduced, thereby resulting in increased oxidative stress.

Ultrastructural analyses revealed mitochondrial abnormalities in 10–20% of AR-deficient myofibres (*Figure S6C*), including megamitochondria with normal cristae density (*Figure 6F*, red arrow), swollen mitochondria with reduced cristae content (*Figure 6F*, blue arrow) and mitochondria devoid of material (*Figure 6F*, white arrow), which might contribute to reduced respiration capacities. Of note, myofibres in which most of the mitochondria were swollen presented nuclear condensation, as well as chromatin clumps and marginalization (*Figures 6F* and *S6C*), which are characteristic of cell necrosis. Histological analyses of transversal muscle sections revealed the presence of <1% of necrotic myofibres (*Figures 6G* and *S6D*), characterized by the expression of

DOI: 10.1002/jcsm.13251

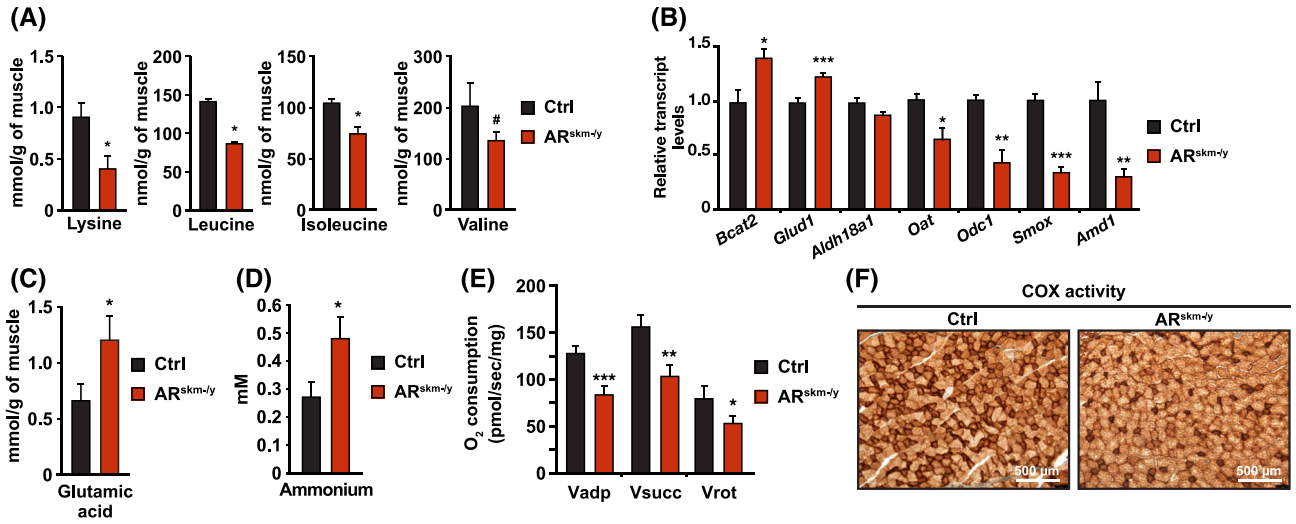

Figure 5 Impact of myofibre androgen receptor (AR) deficiency on amino acid metabolism and mitochondrial functions (see also *Figure S6*). (A) Level of indicated amino acids in gastrocnemius muscles of 15-week-old control (Ctrl) and $AR^{skm-/y}$ mice. n = 3 mice. Mean + SEM. Two-tailed Mann–Whitney test. $^{*}P < 0.05$ and $^{\#}P = 0.1$. (B) Relative transcript levels of the indicated genes in gastrocnemius muscles of 15-week-old Ctrl and $AR^{skm-/y}$ mice. n = 6 mice. Mean + SEM. Two-tailed t-test. $^{*}P < 0.05$, $^{**}P < 0.01$ and $^{***}P < 0.001$. (C, D) Level of glutamic acid (C) and ammonium (D) in gastrocnemius muscles of 15-week-old Ctrl and $AR^{skm-/y}$ mice. (C) n = 3 mice, (D) n = 6 mice. Mean + SEM. (C) Two-tailed Mann–Whitney test. (D) Two-tailed t-test. $^{*}P < 0.05$. (E) Oxygen consumption in saponin-skinned gastrocnemius fibres of 15-week-old Ctrl and $AR^{skm-/y}$ mice in the presence of ADP (Vadp), succinate (Vsucc, maximal respiration) and rotenone (Vrot, respiration via complex II). n = 6 mice. Mean + SEM. Two-tailed t-test. $^{*}P < 0.05$, $^{**}P < 0.01$ and $^{***}P < 0.001$. (F) Representative histochemical staining of COX activity in quadriceps muscle of 15-week-old Ctrl and $AR^{skm-/y}$ mice. Oxidative and intermediate fibres are darkly and moderately stained, respectively; glycolytic fibres are lightly stained. Scale bar: 500 µm. n = 6 mice, 3 fields per mouse.

the necrosis markers PUMA, FADD and RIPK3, associated with infiltration of F4/80-positive macrophages (*Figure 6G*). Various stages of metabolic necrosis were observed: (i) fibres with a pale cytoplasm, (ii) sarcolemma membrane disruptions and (iii) phagocytic necrosis where myofibres are infiltrated by macrophages (*Figures 6G* and *S6D*). DNA fragmentation detection by TUNEL assay confirmed the presence of dying myofibres (*Figure S6E*), but no apoptotic cleaved caspase 3 (CASP3)-positive cells were observed (*Figure S6E*). Note that necrotic fibres and swollen mitochondria were also observed in muscles of $AR^{(i)skm-/y}$ mice lacking AR at adulthood (*Figure S6F,G*), but not in those of $AR^{skm-/-}$ females (*Figure S6H*). Together, these data show that AR loss in muscle fibres leads to increased lysine and BCAA catabolism and decreased polyamine biosynthesis, as well as glutamate, ammonia and ROS accumulation, mitochondrial damages and necrosis of highly affected fibres in male mice.

Androgen receptor controls the expression of numerous transcription factors, metabolic enzymes and structural proteins in myofibres of male mice

To characterize the molecular players that account for the phenotype of $AR^{skm-/y}$ mice, we performed a transcriptomic analysis of gastrocnemius muscles from control and mutant mice at the age of 9 weeks. Our data unravelled 1092 down-regulated and 1046 up-regulated genes in $AR^{skm-/y}$ mice compared with control mice. Pathway analysis revealed that up-regulated genes are involved in amino acid and nitrogen metabolism and in fatty acid beta-oxidation (*Figure 7A*). In agreement with our RT-qPCR and metabolomic analyses, the transcript levels of numerous genes encoding enzymes involved in BCAA and lysine degradation (e.g., *Acaa2*, *Acads*, *Acadsb*, *Aldh7a1*, *Bcat2*, *Bckdhb*, *Dbt*, *Echs1*, *Gcdh*, *Hadha*, *Hadhb* and *Ivd*) and in fatty acid beta-oxidation (e.g., *Acox1*, *Acadl*, *Acads* and *Hadha*) were increased after AR loss in myofibres (*Figures 7B,C* and *S7A–D*). Transcriptomic analysis also confirmed the up-regulation of transcripts encoding enzymes involved in nitrogen metabolism, such as *Glud1* and the glutamate-ammonia ligase *Glul*, as well as the decrease in those encoding enzymes involved the polyamine pathway, such as *Oat*, *Azin2*, *Odc1*, *Amd1*, *Amd2* and *Smox* (*Figures 7D*, *S6B* and *S7E*). These results also unveiled that the transcript levels of the glucocorticoid receptor (*GR*; *Nr3c1*) were increased in muscles in the absence of AR, which was confirmed by RT-qPCR (*Figure S8A*). Pathway analysis revealed that genes down-regulated in $AR^{skm-/y}$ mice are involved in energy metabolism, such as insulin signalling, glycolysis and fatty acid biosynthesis (*Figure 7E*). Transcript levels of the glucose transporter *Glut3* (*Slc2a3*), the main isoform involved in insulin-independent basal glucose uptake into muscles,[29] of various genes involved in anaerobic glycolysis, including *Hk2*, and as well as *Pcx*, which converts pyruvate to oxaloac-

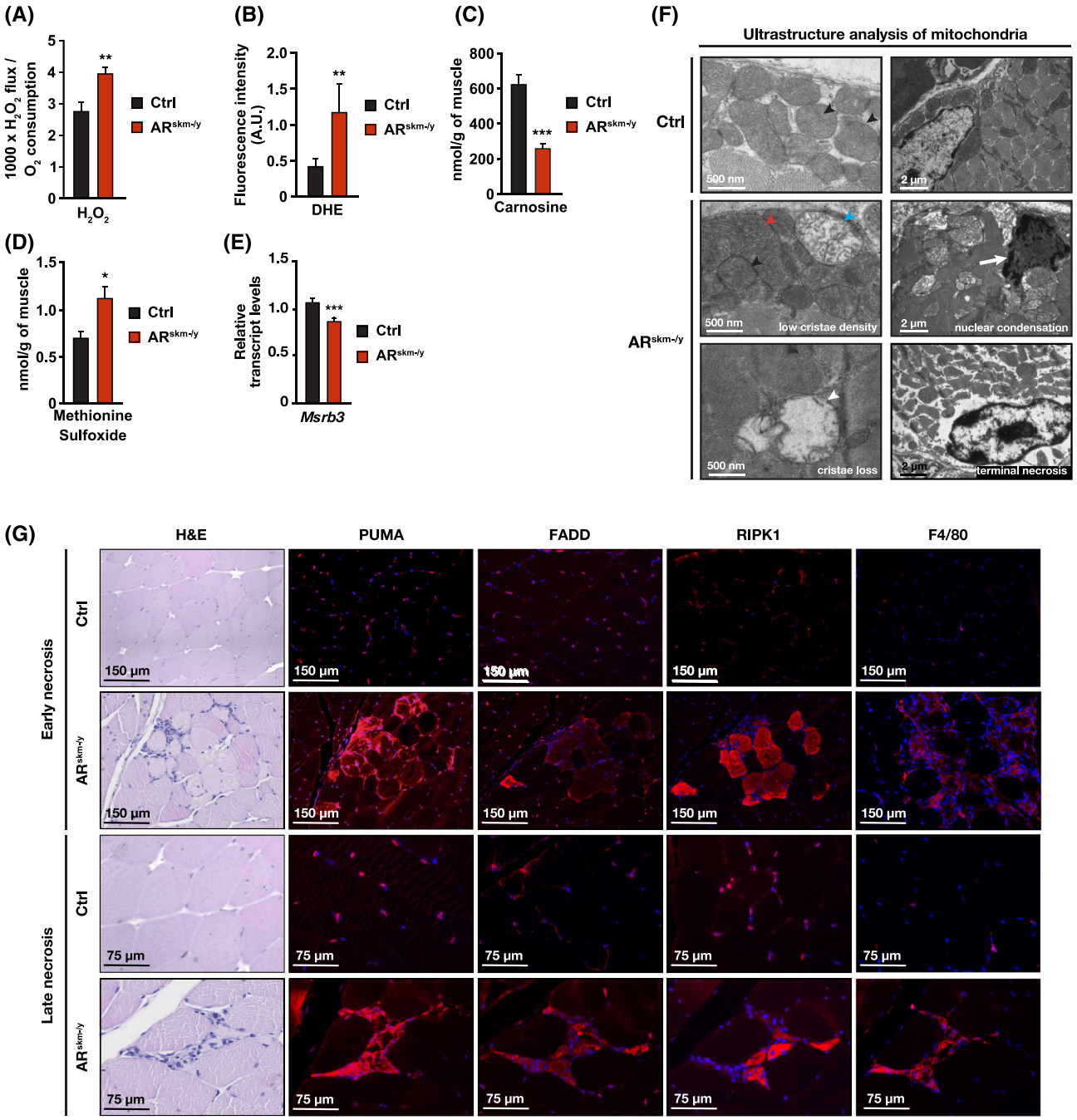

Figure 6 Impact of androgen receptor (AR) deficiency in myofibres on oxidative stress and fibre viability (see also *Figure S6*). (A, B) Measurement of H_2O_2 production relative to oxygen consumption determined in the presence of ADP (A) and fluorescent detection of reactive oxygen species (ROS) production by quantification of dihydroethidium (DHE) staining intensity (B) on gastrocnemius fibres of 15-week-old control (Ctrl) and $AR^{skm-/y}$ mice. n = 6 mice. Mean + SEM. (B) Thirty fields per mouse. Two-tailed t-test. $^{**}P < 0.01$. (C, D) Level of carnosine (C) and methionine sulfoxide (D) in gastrocnemius muscles of 15-week-old Ctrl and $AR^{skm-/y}$ mice. n = 3 mice. Mean + SEM. Two-tailed Mann–Whitney test. $^{*}P < 0.05$ and $^{***}P < 0.001$. (E) Relative *Msrb3* transcript levels in gastrocnemius muscles of 15-week-old Ctrl and $AR^{skm-/y}$ mice. n = 6 mice. Mean + SEM. Two-tailed t-test. $^{***}P < 0.001$. (F) Representative ultrastructure of quadriceps muscle of 15-week-old Ctrl and $AR^{skm-/y}$ mice. Black, red, blue and white arrowheads show normal mitochondria, megamitochondria, mitochondria swelling and cristae loss, respectively; white arrow shows necrotic nucleus. Scale bar: 500 nm and 2 µm, as indicated. n = 10 mice, 10 fields per mouse. (G) Representative haematoxylin and eosin (H&E) staining, and PUMA, FADD, RIPK1 and F4/80 immunofluorescent detection with DAPI-stained nuclei of quadriceps muscles of 15-week-old Ctrl and $AR^{skm-/y}$ mice. Scale bars: 75 and 150 µm, as indicated. n = 5 mice, 10 fields per mouse.

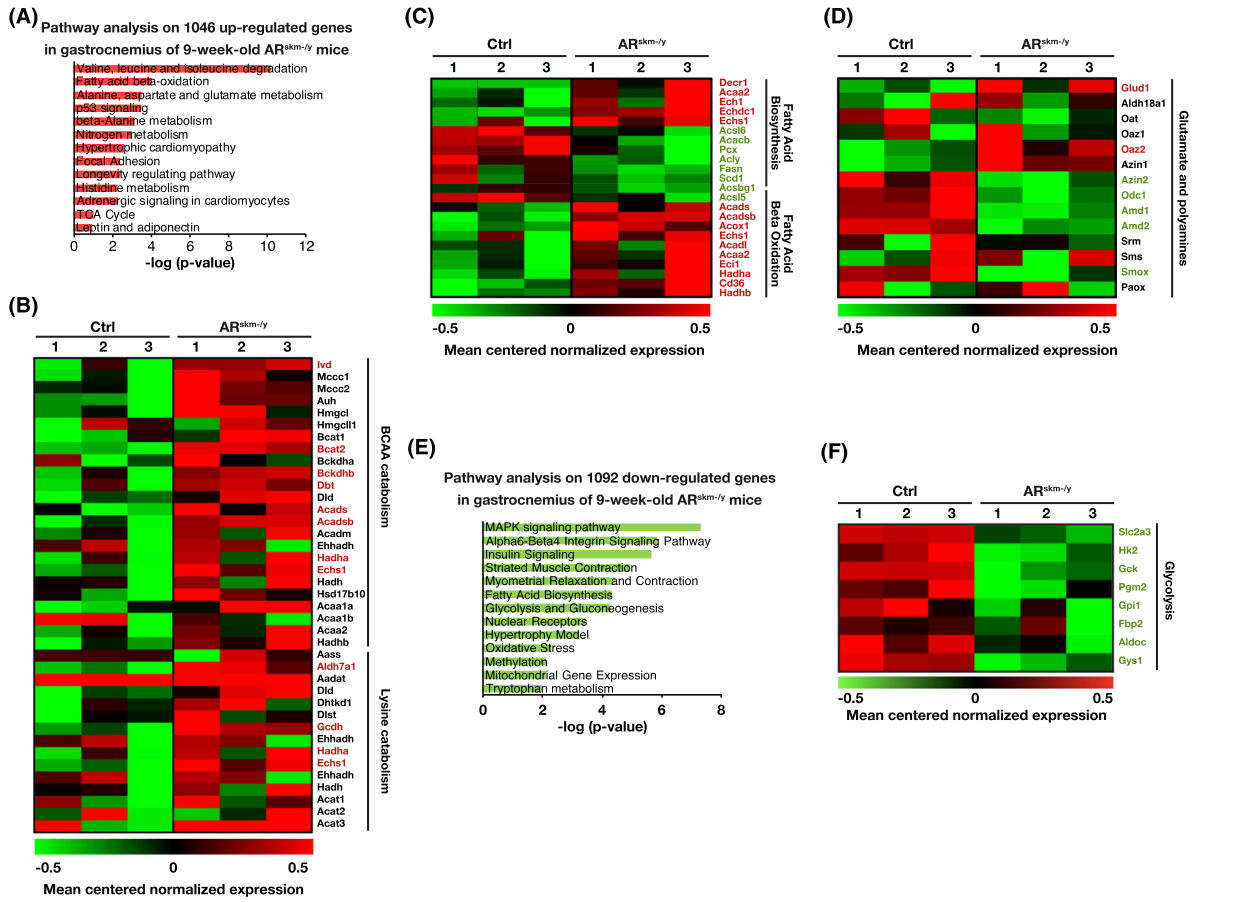

Figure 7 Analysis of androgen receptor (AR) functional targets in skeletal muscle (see also *Figures S7* and *S8*). (A) Pathway analysis of genes up-regulated in gastrocnemius muscle of 9-week-old AR$^{skm-/y}$ mice. (B–D) Heatmap depicting the mean centred normalized expression of genes involved in branched-chained amino acid (BCAA) and lysine metabolism (B), fatty acid synthesis and beta-oxidation (C), glutamine and polyamine metabolism (D), obtained by RNA-seq analysis performed on gastrocnemius muscle of 9-week-old control (Ctrl) and AR$^{skm-/y}$ mice. Genes significantly up-regulated and down-regulated in AR$^{skm-/y}$ mice are marked in red and green, respectively. (E) Pathway analysis of genes down-regulated in gastrocnemius muscle of 9-week-old AR$^{skm-/y}$ mice. (F) Heatmaps depicting the mean centred normalized expression of genes involved in glycolysis obtained by RNA-seq analysis performed on gastrocnemius muscle of 9-week-old Ctrl and AR$^{skm-/y}$ mice. Genes significantly down-regulated in AR$^{skm-/y}$ mice are marked in green.

etate, were decreased (*Figures 7C,F* and *S8A,B*), thereby showing that AR is instrumental for pyruvate entry in the TCA cycle. Furthermore, transcript levels of genes encoding enzymes promoting de novo fatty acid synthesis, including *Acly*, *Scd1* and *Fasn*, were decreased in the absence of myofibre AR (*Figures 7C* and *S8C*).

Importantly, transcriptomic data also revealed that *Lmod1*, *Lmod3*, *Tcap* and *Tnni2*, encoding proteins of the contractile cytoskeleton, and numerous genes involved in muscle non-contractile cytoskeleton were down-regulated in AR$^{skm-/y}$ mice, including the ryanodine receptor 1 (*Ryr1*), dystrophin (*Dmd*), desmin (*Des*), myozenin 1 (*Myoz1*), gamma filamin (*Flnc*), misshapen-like kinase 1 (*Mink1*), myopodin (*Synpo2*), dystrobrevin beta (*Dtnb*) and caveolin 3 (*Cav3*) (*Figure S8D*), whereas the transcript levels of titin (*Ttn*), myosins (*Myh*), troponins (*Tnnt*) and tropomyosins (*Tpm*) encoding structural muscle proteins were not affected (*Figure S8E*). These results were corroborated by RT-qPCR analyses in gastrocnemius of 15-week-old AR$^{skm-/y}$ and AR$^{(i)skm-/y}$ mice (*Figure S8F,G*).

To identify direct AR targets, hind limb muscle chromatin from 11-week-old mice was immunoprecipitated with antibodies directed against AR, followed by massive parallel sequencing (ChIP-seq), together with a characterization of dimethylated lysine 4 from histone H3 (H3K4me2) chromatin occupancy as a hallmark of active promoters and enhancers. Bioinformatics analysis uncovered 4691 AR peaks, mainly located at intronic and intergenic regions, and 47 225 H3K4me2 peaks (*Figures 8A* and *S9A*). An analysis of AR genomic distribution revealed that peaks were present in far upstream and downstream regions (−100 to −50 kb and 50 to 100 kb), intermediate locations (−50 to −20 kb and 20

to 50 kb) and DNA segments in the vicinity of the transcription start site (TSS) (−10 to −2 kb, −2 to 2 kb and 2 to 10 kb) (*Figure S9B*). HOMER motif search unveiled that AR is recruited to DNA via androgen response elements (AREs; 2.5%, *P* = 1e-11), AR half-sites (37.6%, *P* = 1e-24) and oxosteroid response elements identified as progesterone response elements (PREs; 23.3%, *P* = 1e-40) (*Figure 8B*). The list of AR peaks containing the oxosteroid response element 5′-RGRACAnnnTGTYCY-3′ and cognate target genes (e.g., *Acat1*, *Adcy8*, *Igf1*, *Lamb1*, *Mmd*, *Nrf1*, *Phkb*, *Serpina3a*, *Serpinb9d*, *Slc4a2* and *Tlr4*) is provided in *Table S2*. Approximately 15% of the genes down-regulated in muscles of $AR^{skm-/y}$ mice were bound by AR as determined by a nearest TSS analysis (*Figure S9C*), including *Dmd* and *Odc1* (*Table S2*). A gene centric analysis using TSS coordinates showed that AR is recruited to 88 out of 1092 genes down-regulated in $AR^{skm-/y}$ mice within a 2-kb window and to 657 within a 200-kb window (*Figure 8C* and *Table S2*), indicating that AR modulates target gene expression mainly via enhancers located at far upstream or downstream regions. We found that AR directly controls numerous genes involved in metabolic processes, including glycolysis (e.g., *Fbp2*, *Gpi1*, *Mpc1*, *Pcx* and *Pfkfb3*), lipid metabolism (e.g., *Aacs*, *Acat1*, *Acbd4*, *Acly*, *Acot7*, *Adcy8*, *Dagla*, *Fasn*, *Mfn2* and *Scd1*) and polyamine biosynthesis (e.g., *Amd1*, *Amd2*, *Odc1* and *Smox*) (*Figures 8D* and *S9D* and *Table S2*). Our analysis also unveiled that AR controls the expression of many genes involved in muscle contraction, including *Lmod1*, *Lmod3*, *Tcap* and *Tnni2* of the contractile cytoskeleton; *Cav3*, *Col17a1* and *Dtnb* of the non-contractile cytoskeleton; *Itgb4*, *Itgb5* and *Itgb7* of the extracellular matrix; *Mylk4* and *Myom1* that contribute to muscle strength; and *Cacnai* and *Cacng7* encoding subunits of calcium voltage-gated channels, also known as dihydropyridine receptors (DHPRs) (*Table S2*). Immunofluorescent analysis on longitudinal tibialis sections revealed that DHPR beta (DHPRB) and the sarcoplasmic reticulum Ca^{2+} transport ATPase SERCA1 were expressed in both control and $AR^{skm-/y}$ mice, whereas DHPR alpha (DHPRA) and RYR1 were hardly detectable in the absence of myofibre AR (*Figures 8E* and *S9E*). Moreover, this analysis unveiled structural alterations in the sarcoplasmic reticulum (*Figures 8E* and *S9E*). Ultrastructural analyses revealed T-tubules dilatation and misalignment to the Z-lines in 10–20% of AR-null myofibres (*Figure 8F*), indicating an altered connection between sarcolemma and endoplasmic reticulum that might affect calcium signalling.

In addition, we identified various transcription factors and co-regulators as direct targets of AR in skeletal muscle, which were down-regulated in AR-deficient myofibres (e.g., *Atf4*, *Cux2*, *Irx3*, *Nrf1*, *Pgc1a*, *Trp53*, *Trp63*, *Smyd2*, *Med25* and *Smarca2*; the nuclear receptors *Nr1d1* [*Rev-ErbAlpha*], *Rarb*, *Rorc* and *Thra*; and *Myod1*, *Naca*, *Tcf15* and *Tead4*, which modulate muscle development) (*Figure S9D* and *Table S2*).

Altogether, these combined cistromic and transcriptomic analyses show that myofibre AR directly controls the expression of a number of transcription factors and numerous genes involved in glycolysis, fatty acid processing, polyamine biosynthesis and ROS scavenging, as well as various components of skeletal muscle cytoskeleton (*Figure S10*).

Discussion

To date, the molecular and cellular mechanisms underlying androgen tissue-selective effects remain elusive. By analysing $AR^{skm-/y}$ mice, we demonstrate that AR modulates metabolic characteristics of male skeletal muscles. Our combined mouse and tissue culture studies show that AR loss in myofibres leads to decreased glucose uptake and glycolytic activity, and to premature development of type 2 diabetes.

Previous studies showed that DHT promotes the expression of glycolytic genes in various cell types, including *Hk2* and *Pfk2* in cardiomyocytes,[30] increases GLUT4 (SLC2A4) protein expression and translocation, as well as PFK and HK activities in muscle cell lines,[11] and stimulates *Slc2a3* and *Hk2* expression in skeletal muscles of female mice.[31] However, none of the corresponding genes was identified as a direct AR target in muscles to our knowledge. Our cistromic analysis uncovered that numerous genes involved in glucose metabolism, including *Fbp2*, *Pcx* and *Pfkfb3*, are direct AR targets. Because AR ablation in myofibres of adult male mice also impaired glucose homeostasis, AR promotes glucose usage in mature myofibres. In addition to impaired glucose metabolism, fatty acids were less efficiently metabolized in skeletal muscles of $AR^{skm-/y}$ mice. Indeed, notwithstanding increased transcript levels of the fatty acid transporter *Cd36* and of genes encoding key enzymes of beta-oxidation, as well as mitochondrial content in $AR^{skm-/y}$ mice, LPL activity and mitochondrial respiration were strongly diminished, and lipid droplets accumulated in AR-depleted muscles. Interestingly, we identified *Pgc1a* and *Nrf1*, two major coordinators of muscle oxidative metabolism and mitochondrial activity,[32] as direct AR targets. Their reduced expression might contribute to decreased oxidative phosphorylation in AR-deficient fibres. However, whereas fatty acid oxidation is androgen dependent in prostate cancer cells,[33] the expression of genes encoding enzymes of beta-oxidation was enhanced in the absence of AR in myofibres, which highlights cell-specific androgen activities.

In addition, our various molecular analyses show that the expression of numerous genes encoding enzymes involved in BCAA and lysine degradation was up-regulated in skeletal muscles of $AR^{skm-/y}$ mice, in accordance with previous results,[31] resulting in decreased levels of these amino acids in their myofibres. As these genes have been shown to be activated by glucocorticoid pathways,[34] and as GR transcript levels were enhanced in $AR^{skm-/y}$ mice, GR-dependent transcription might contribute to increased levels of BCAA degra-

DOI: 10.1002/jcsm.13251

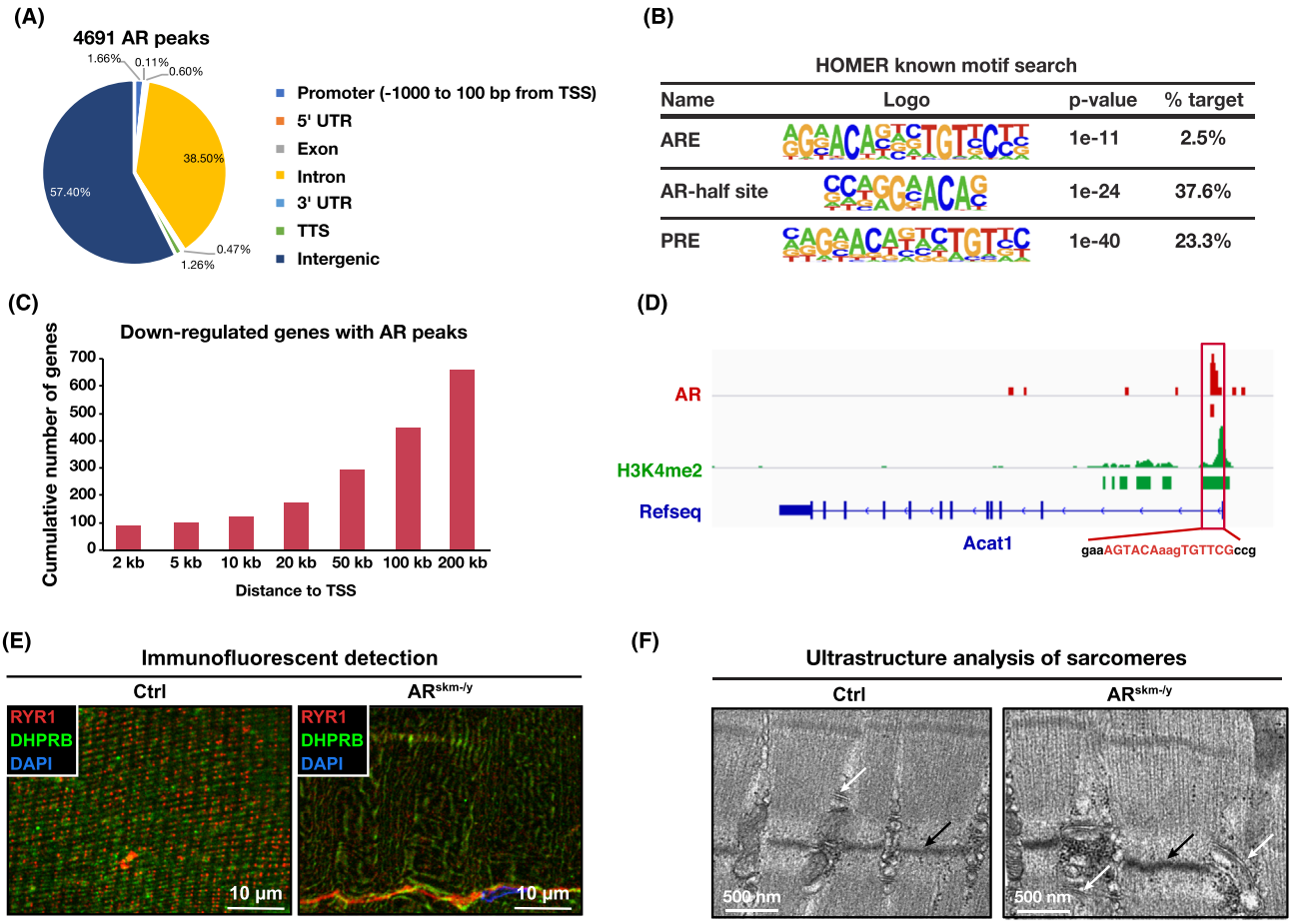

Figure 8 Characterization of androgen receptor (AR) cistrome in skeletal muscle (see also *Figure S9*). (A) Pie chart depicting the AR peak distribution in the genome of skeletal muscles. TSS, transcription start site; TTS, transcription termination site; UTR, untranslated region. (B) HOMER known motif analysis of AR-bound DNA sequences in skeletal muscles. (C) Cumulative number of genes down-regulated in $AR^{skm-/y}$ mice with an AR peak at indicated distances from their TSS. (D) Localization of AR and H3K4me2 at the *Acat1* locus. The AR-response element is shown in red. (E) Representative immunofluorescent detection of the RYR1 (red) and DHPRB (green) in tibialis muscles of 15-week-old control (Ctrl) and $AR^{skm-/y}$ mice. Nuclei are stained with DAPI. Scale bar: 10 µm. *n* = 4 mice, 3 fields per mouse. (F) Representative ultrastructure of tibialis sarcomeres from 15-week-old Ctrl and $AR^{skm-/y}$ mice. White arrow points to a T-tubule. Black arrows show the Z-line. Scale bar: 500 nm. *n* = 10 mice, 10 fields per mouse.

dation enzymes in $AR^{skm-/y}$ mice, and it is therefore unlikely that AR directly represses the expression of enzymes involved in BCAA catabolism. Thus, our results show that glycolytic flux and fatty acid usage are reduced in AR-deficient myofibres of male mice. In contrast, catabolism of BCAA and lysine, which reside as a pool of consumable amino acids in myofibres, is enhanced to produce acetyl-CoA that fuels the TCA cycle, probably as a compensatory mechanism that is sufficient to sustain basal muscle activities, without impacting muscle proteins.

In addition to the metabolic defects, our combined immunofluorescent and ultrastructural analyses revealed sarcoplasmic reticulum abnormalities in $AR^{skm-/y}$ muscles. We and others previously showed that limb muscle strength was reduced in skeletal muscle-specific AR knockout mice.[17,18,35,36] We also demonstrated that myofibrils were disrupted in ~10% of the sarcomeres from $AR^{skm-/y}$ mice, with loss of myofilaments, rupture of Z-lines and enlarged sarcoplasm.[17] Our omics data now unveil that AR directly controls the expression of numerous genes of the contractile cytoskeleton and the calcium channel subunits. As calcium flux stimulates aerobic metabolism and ATP production,[37] impaired calcium conduction caused by decreased expression of calcium channel subunits and triad disorganization might contribute to mitochondrial dysfunction in $AR^{skm-/y}$ mice. Furthermore, in concordance with others,[10,31] we identified several genes involved in polyamine synthesis as AR targets in skeletal muscles. Even though polyamines were proposed

as androgen-induced anabolic agents,[38] spermidine supplementation in orchiectomized mice was not sufficient to improve their muscle mass and strength.[39] Our data indicate that decreased levels of enzymes interconverting polyamines and increased transcript levels of *Glud1* in skeletal muscles of $AR^{skm-/y}$ mice lead to higher glutamate levels. Moreover, enhanced ammonia levels in $AR^{skm-/y}$ skeletal muscles, resulting from increased BCAA catabolism, might contribute to impaired skeletal muscle mitochondrial respiration and oxidative stress. Therefore, impaired calcium conduction, increased ammonia production and decreased *Pgc1a* and *Nrf1* levels altogether lead to the mitochondrial alterations of $AR^{skm-/y}$ myofibres, which, along with decreased expression and disorganization of the cytoskeleton elements, impacts muscle function. In contrast, myofibre integrity and glucose homeostasis were not affected in female mice lacking myofibre AR at endogenous androgen levels.

Our findings also provide important insights in diseases caused by impaired AR function. Indeed, patients with Kennedy's disease (KD), also known as spinal and bulbar muscular atrophy (SBMA), an X-linked recessive neuromuscular disease induced by glutamine expansions in the AR N-terminal region, suffer from metabolic alterations (e.g., glucose intolerance),[40] reduced muscle force, associated with disrupted muscle striation, and altered calcium dynamics in response to muscle contraction.[41,42] Corresponding poly-Q expansions in mice impaired glycolysis with decreased HK2 expression and altered mitochondrial functions in their muscles,[43] as in $AR^{skm-/y}$ mice. Thus, defects induced by the poly-Q-AR might be due to impaired AR transcriptional activity in skeletal muscle rather than toxicity of the misfolded protein. Because liver and adipose tissues are also important metabolic organs, impaired AR activity in these tissues might contribute to the phenotype of KD patients.

In summary, our comprehensive study delineates the mechanisms by which androgens, via their receptor in myofibres, control male muscle mechanical and energetic functions, as well as whole-body glucose metabolism. Unravelling androgen signalling in additional target tissues will open new avenues to develop AR ligands with increased selective activities for the treatment of various diseases.

Acknowledgements

This work of the Interdisciplinary Thematic Institute IMCBio, as part of the ITI 2021–2028 programme of the University of Strasbourg, the Centre national de la recherche scientifique (CNRS) and the Institut national de la santé et de la recherche médicale (Inserm), was supported by Agence Nationale de la Recherche (ANR) with the IdEx Unistra (ANR-10-IDEX-0002), SFRI-STRAT'US (ANR 20-SFRI-0012) and EUR IMCBio (ANR-17-EURE-0023) projects, under the framework of the French Investments for the Future Programme. Additional funding was delivered by Inserm, CNRS, the University of Strasbourg, IGBMC, ANR (ANR-10-BLAN-1108, AndroGluco, ANR-16-CE11-0009, AR2GR), AFM-Téléthon (Strategic Programme 15352), Inserm young researcher grant (to D.D.), and ANR-10-LABX-0030-INRT, a French State fund managed by the ANR under the frame programme Investissements d'Avenir (ANR-10-IDEX-0002-02). A.-I.R. was supported by LabEx INRT funds, D.R. by ANR (ANR-16-CE11-0009, AR2GR), M.S. by AFM (15352), K.G. by the Association pour la Recherche à l'IGBMC (ARI), C.C. by AFM and ARI, J.R. by the Programme CDFA-07-22 from the Université franco-allemande and Ministère de l'Enseignement Supérieur de la Recherche et de l'Innovation and Q.C. by ANR (ANR-20-CE14-0040-01). Funding for open access charge was provided by ANR. We are grateful to Jean-Marc Bornert and Anastasia Bannwarth for providing excellent technical assistance. We thank the IGBMC animal house, cell culture and imaging facilities, the Mouse Clinical Institute (ICS, Illkirch, France) and the GenomEast platform, a member of the 'France Génomique' consortium (ANR-10-INBS-0009) for support. We acknowledge Pr. S. Kato for floxed AR mice.

Conflict of interest statement

None declared.

Online supplementary material

Additional supporting information may be found online in the Supporting Information section at the end of the article.

References

1. Schiaffino S. Fibre types in skeletal muscle: a personal account. *Acta Physiol (Oxf)* 2010;**199**:451–463.
2. Handschin C, Chin S, Li P, Liu F, Maratos-Flier E, LeBrasseur NK, et al. Skeletal muscle fiber-type switching, exercise intolerance, and myopathy in PGC-1α muscle-specific knock-out animals. *J Biol Chem* 2007;**282**:30014–30021.
3. Figueiredo PA, Powers SK, Ferreira RM, Amado F, Appell HJ, Duarte JA. Impact of lifelong sedentary behavior on mitochondrial function of mice skeletal muscle. *J Gerontol A Biol Sci Med Sci* 2009;**64**: 927–939.
4. Porter C, Hurren NM, Cotter MV, Bhattarai N, Reidy PT, Dillon EL, et al. Mitochondrial respiratory capacity and coupling control

decline with age in human skeletal muscle. *Am J Physiol Endocrinol Metab* 2015;**309**: E224–E232.
5. Duteil D, Chambon C, Ali F, Malivindi R, Zoll J, Kato S, et al. The transcriptional coregulators TIF2 and SRC-1 regulate energy homeostasis by modulating mitochondrial respiration in skeletal muscles. *Cell Metab* 2010;**12**:496–508.
6. Haizlip KM, Harrison BC, Leinwand LA. Sex-based differences in skeletal muscle kinetics and fiber-type composition. *Physiology (Bethesda)* 2015;**30**:30–39.
7. Kuo T, Harris CA, Wang JC. Metabolic functions of glucocorticoid receptor in skeletal muscle. *Mol Cell Endocrinol* 2013;**380**: 79–88.
8. Nicolaisen TS, Klein AB, Dmytriyeva O, Lund J, Ingerslev LR, Fritzen AM, et al. Thyroid hormone receptor α in skeletal muscle is essential for T3-mediated increase in energy expenditure. *FASEB J* 2020;**34**:15480–15491.
9. Ueberschlag-Pitiot V, Stantzou A, Messéant J, Lemaitre M, Owens DJ, Noirez P, et al. Gonad-related factors promote muscle performance gain during postnatal development in male and female mice. *Am J Physiol Endocrinol Metab* 2017;**313**: E12–E25.
10. MacLean HE, Chiu WSM, Notini AJ, Axell AM, Davey RA, McManus JF, et al. Impaired skeletal muscle development and function in male, but not female, genomic androgen receptor knockout mice. *FASEB J* 2008;**22**:2676–2689.
11. Sato K, Iemitsu M, Aizawa K, Ajisaka R. Testosterone and DHEA activate the glucose metabolism-related signaling pathway in skeletal muscle. *Am J Physiol Endocrinol Metab* 2008;**294**:E961–E968.
12. Lubahn DB, Joseph DR, Sullivan PM, Willard HF, French FS, Wilson EM. Cloning of human androgen receptor complementary DNA and localization to the X chromosome. *Science* 1988;**240**:327–330.
13. Swift-Gallant A, Monks DA. Androgen receptor expression in satellite cells of the neonatal levator ani of the rat. *Dev Neurobiol* 2013;**73**:448–454.
14. van Anders SM, Steiger J, Goldey KL. Effects of gendered behavior on testosterone in women and men. *Proc Natl Acad Sci U S A* 2015;**112**:13805–13810.
15. Fernando SM, Rao P, Niel L, Chatterjee D, Stagljar M, Monks DA. Myocyte androgen receptors increase metabolic rate and improve body composition by reducing fat mass. *Endocrinology* 2010;**151**:3125–3132.
16. Kim J, Park J, Kim N, Park HY, Lim K. Inhibition of androgen receptor can decrease fat metabolism by decreasing carnitine palmitoyltransferase I levels in skeletal muscles of trained mice. *Nutr Metab (Lond)* 2019;**16**:82.
17. Chambon C, Duteil D, Vignaud A, Ferry A, Messaddeq N, Malivindi R, et al. Myocytic androgen receptor controls the strength but not the mass of limb muscles. *Proc Natl Acad Sci U S A* 2010;**107**:14327–14332.
18. Ophoff J, van Proeyen K, Callewaert F, de Gendt K, de Bock K, vanden Bosch A, et al. Androgen signaling in myocytes contributes to the maintenance of muscle mass and fiber type regulation but not to muscle strength or fatigue. *Endocrinology* 2009;**150**:3558–3566.
19. Yu JG, Bonnerud P, Eriksson A, Stål PS, Tegner Y, Malm C. Effects of long term supplementation of anabolic androgen steroids on human skeletal muscle. *PLoS ONE* 2014;**9**:e105330.
20. De Gendt K, Verhoeven G. Tissue- and cell-specific functions of the androgen receptor revealed through conditional knockout models in mice. *Mol Cell Endocrinol* 2012;**352**:13–25.
21. Shiina H, Matsumoto T, Sato T, Igarashi K, Miyamoto J, Takemasa S, et al. Premature ovarian failure in androgen receptor-deficient mice. *Proc Natl Acad Sci U S A* 2006;**103**:224–229.
22. Miniou P, Tiziano D, Frugier T, Roblot N, le Meur M, Melki J. Gene targeting restricted to mouse striated muscle lineage. *Nucleic Acids Res* 1999;**27**:27e.
23. Schuler M, Ali F, Metzger E, Chambon P, Metzger D. Temporally controlled targeted somatic mutagenesis in skeletal muscles of the mouse. *Genesis* 2005;**41**:165–170.
24. Hoehn KL, Turner N, Swarbrick MM, Wilks D, Preston E, Phua Y, et al. Acute or chronic upregulation of mitochondrial fatty acid oxidation has no net effect on whole-body energy expenditure or adiposity. *Cell Metab* 2010;**11**:70–76.
25. Kamei Y, Hatazawa Y, Uchitomi R, Yoshimura R, Miura S. Regulation of skeletal muscle function by amino acids. *Nutrients* 2020;**12**:261.
26. Chattopadhyay MK, Tabor H. Polyamines are critical for the induction of the glutamate decarboxylase-dependent acid resistance system in *Escherichia coli*. *J Biol Chem* 2013;**288**:33559–33570.
27. Mann G, Mora S, Madu G, Adegoke OAJ. Branched-chain amino acids: catabolism in skeletal muscle and implications for muscle and whole-body metabolism. *Front Physiol* 2021;**12**:702826.
28. Davuluri G, Allawy A, Thapaliya S, Rennison JH, Singh D, Kumar A, et al. Hyperammonaemia-induced skeletal muscle mitochondrial dysfunction results in cataplerosis and oxidative stress. *J Physiol* 2016;**594**:7341–7360.
29. Copland JA, Pardini AW, Wood TG, Yin D, Green A, Bodenburg YH, et al. IGF-1 controls GLUT3 expression in muscle via the transcriptional factor Sp1. *Biochim Biophys Acta* 2007;**1769**:631–640.
30. Troncoso MF, Pavez M, Wilson C, Lagos D, Duran J, Ramos S, et al. Testosterone activates glucose metabolism through AMPK and androgen signaling in cardiomyocyte hypertrophy. *Biol Res* 2021;**54**:3.
31. Sakakibara I, Yanagihara Y, Himori K, Yamada T, Sakai H, Sawada Y, et al. Myofiber androgen receptor increases muscle strength mediated by a skeletal muscle splicing variant of Mylk4. *iScience* 2021;**24**:102303.
32. Schuler M, Ali F, Chambon C, Duteil D, Bornert JM, Tardivel A, et al. PGC1α expression is controlled in skeletal muscles by PPARβ, whose ablation results in fiber-type switching, obesity, and type 2 diabetes. *Cell Metab* 2006;**4**:407–414.
33. Mah CY, Nassar ZD, Swinnen JV, Butler LM. Lipogenic effects of androgen signaling in normal and malignant prostate. *Asian J Urol* 2020;**7**:258–270.
34. Liu Y, Dong W, Shao J, Wang Y, Zhou M, Sun H. Branched-chain amino acid negatively regulates KLF15 expression via PI3K-AKT pathway. *Front Physiol* 2017;**8**:853.
35. Fraysse B, Vignaud A, Fane B, Schuh M, Butler-Browne G, Metzger D, et al. Acute effect of androgens on maximal force-generating capacity and electrically evoked calcium transient in mouse skeletal muscles. *Steroids* 2014;**87**:6–11.
36. Rana K, Chiu MWS, Russell PK, Skinner JP, Lee NKL, Fam BC, et al. Muscle-specific androgen receptor deletion shows limited actions in myoblasts but not in myofibers in different muscles in vivo. *J Mol Endocrinol* 2016;**57**:125–138.
37. Griffiths EJ, Rutter GA. Mitochondrial calcium as a key regulator of mitochondrial ATP production in mammalian cells. *Biochim Biophys Acta* 2009;**1787**: 1324–1333.
38. Lee NK, MacLean HE. Polyamines, androgens, and skeletal muscle hypertrophy. *J Cell Physiol* 2011;**226**:1453–1460.
39. Gordon BS, Rossetti ML, Casero RA Jr. Spermidine is not an independent factor regulating limb muscle mass in mice following androgen deprivation. *Appl Physiol Nutr Metab* 2021;**46**:452–460.
40. Pradat PF, Bernard E, Corcia P, Couratier P, Jublanc C, Querin G, et al. The French national protocol for Kennedy's disease (SBMA): consensus diagnostic and management recommendations. *Orphanet J Rare Dis* 2020;**15**:90.
41. Rocchi A, Milioto C, Parodi S, Armirotti A, Borgia D, Pellegrini M, et al. Glycolytic-to-oxidative fiber-type switch and mTOR signaling activation are early-onset features of SBMA muscle modified by high-fat diet. *Acta Neuropathol* 2016;**132**:127–144.
42. Chivet M, Marchioretti C, Pirazzini M, Piol D, Scaramuzzino C, Polanco MJ, et al. Polyglutamine-expanded androgen receptor alteration of skeletal muscle homeostasis and myonuclear aggregation are affected by sex. *Age Muscle Metab Cells* 2020;**9**.
43. Giorgetti E, Yu Z, Chua JP, Shimamura R, Zhao L, Zhu F, et al. Rescue of metabolic alterations in AR113Q skeletal muscle by peripheral androgen receptor gene silencing. *Cell Rep* 2016;**17**:125–136.